Published in final edited form as:
Nano Lett. 2009 March ; 9(3): 1139–1146. doi:10.1021/nl8036905.

Experimental and theoretical studies of light-to-heat conversion and collective heating effects in metal nanoparticle solutions

Hugh H. Richardson[1,*], **Michael T. Carlson**[1], **Peter J. Tandler**[2], **Pedro Hernandez**[3], and **Alexander O. Govorov**[3,*]

1 *Department of Chemistry and Biochemistry, Ohio University, Athens, Ohio 45701*

2 *Devision of Math and Science, Walsh University, North Canton, Ohio 44720*

3 *Department of Physics and Astronomy, Ohio University, Athens, Ohio 45701*

Abstract

We perform a set of experiments on photo-heating in a water droplet containing gold nanoparticles (NPs). Using photo-calorimetric methods, we determine efficiency of light-to-heat conversion (η) which turns out to be remarkable close to 1, (0.97< η <1.03). Detailed studies reveal a complex character of heat transfer in an optically-stimulated droplet. The main mechanism of equilibration is due to convectional flow. Theoretical modeling is performed to describe thermal effects at both nano- and millimeter-scales. Theory shows that the collective photo-heating is the main mechanism. For a large concentration of NPs and small laser intensity, an averaged temperature increase (at the millimeter-scale) is significant (~ 7 °C) whereas, on the nanometer scale, the temperature increase at the surface of a single NP is small (0.02 °C). In the opposite regime, a small NP concentration and intense laser irradiation, we find an opposite pictures: a temperature increase at the millimeter-scale is small (0.1 °C) but a local, nanoscale temperature has strong local spikes at the surfaces of NPs (3 °C). These studies are crucial for the understanding of photo-thermal effects in NPs and for their potential and current applications in nano-and bio -technologies.

Introduction

The optical properties of nanoparticles (NPs), including both semiconductor[1, 2] and metal [3–7] nanocrystals, have been studied intensively. Recently, another related physical property – heat generation by NPs under optical illumination (nanoheaters) – has attracted much interest [8–25]. The heat generation from these nanoheaters involves not only absorption of incident photons, but also the conversion of photon energy into heat energy as well as heat transfer from the NP to the surrounding matrix.

Biomedical applications involving nanoheaters rely on a simply mechanism [12, 13, 16, 21, 26–37]. First, the NPs become attached to targeted biological centers such as tumor cells using selective bio-molecular linkers. Then, heat is generated remotely by optically-stimulating the NPs. Finally, the heat generation causes an actuation of a biological process. Some applications that involve the optical and heat generation properties of metal NPs include biological imaging and detection of DNA, RNA and proteins[1, 13, 34, 38–43], drug delivery[44–46] as well as treatment of diseases (photo-thermal cancer therapy[6, 13, 16, 33, 34, 47, 48]).

*Authors to whom correspondence should be addressed; electronic mail: E-mail: richards@helios.phy.ohiou.edu, E-mail: govorov@helios.phy.ohiou.edu.

The important physical property of nanoheaters for current applications in nano-medicine is the increased temperature change of the NP within a biological system [13, 27, 37] and the scope and length over which this temperature change occurs. Some measurements have been made to directly measure the temperature on the surface of Au NPs when optically excited[10, 12, 15, 49, 50]. The heating effect is especially strong for metal NPs since they have many mobile electrons and becomes strongly enhanced when the laser frequency hits the collective plasmon resonance of a NP. Because metal NPs have a very low optical quantum yield (i.e. they are very poor light emitters), the total amount of heat generated is expected to be related to the total optical absorption rate in a relatively simple and straightforward way. Energy balance arguments would suggest that if the optical quantum yield of NPs is very low (10^{-6})[51] then there should be a near unity conversion of photon energy into heat[3, 10, 15, 49, 51, 52]. In contrast to this viewpoint, a recent paper suggests that the efficiency of transducing incident resonant light to heat for a suspension of 20 nm Au NPs is small (less than 5%) and can be increase to by modulating the continuous wave (CW) laser light.[53] In this paper we measured the temperature change in a water droplet containing a colloidal suspension of 20 nm Au NPs after CW laser excitation at 532 nm. The steady-state temperature is in the interval $28.75\ ^\circ C<\Delta T<29.25\ ^\circ C$. Using the measured droplet volume of 0.0035 cm^3, the rate constant for heat dissipation from the droplet (B) of 0.120 s^{-1}, and the laser power (I) of 0.28W, the transduction efficiency (η) of converting absorbed light energy into heat is within the interval of $0.97<\eta<1.03$. The calculated η is remarkably close to 1, as expected for small NPs and is invariant to laser modulation. We are able to model the temperature distribution inside the water droplet after laser excitation and find that, on the nanoscale, the temperature profile has small "bumps" in temperature located around single optically-stimulated NPs but that overall increase in the temperature of the droplet is due to a collective heating effect of many NPs. We further predict that if the particle density is reduced and a larger laser flux is used, large temperature spikes should be observed around the NPs (~3 °C) with little change in the ambient temperature (~0.2 °C).

Experimental

The experimental apparatus can be divided into two main components: the syringe system and the data collection devices. The syringe system consists of the syringe and needle (1 mL, G 3/8 intradermal bevel needle, Becton Dickinson & Co., Franklin Lakes, NJ), a mechanical chopper fabricated in-house, and a CW 532 nm laser (Millenia Vs, Spectra-Physics, Mt. View, CA). A power meter (TPM-300CE, Gentec Electro-Optics, Quebec, Canada) was used to measure and verify the power of the laser. The data collection devices consist of two subsystems: the voltage vs. time data collection system and the optical video collection system. The voltage vs. time data collection system consists of the K-type thermocouple (0.003″ wires, Omega Engineering, Stamford, CT), the thermocouple-to-analog connector (Super MCJ, Omega Engineering), and the data logger (Xplorer GLX, PASCO, Roseville, CA). The thermocouple was fastened onto the sides of the syringe using hot glue and positioned so the bead was directly adjacent to the needle tip without contact. The optical video collection system consists of a digital camera (Coolpix 885, Nikon) connected to an eyepiece of a 10 × magnification microscope, a monitor (Trinitron, Sony), and a DVD video recorder (D-R410, Toshiba).

The experiment proceeded as follows: The laser was turned on and allowed to warm up. The syringe was filled with a gold colloid solution. (Fabricated by British Biocell International and purchased from Ted Pella, the 20 nm Au colloid was diluted to a 1:11 ratio with Millipore 18 MΩ distilled, deionized water resulting in a concentration of 7×10^{10} particles/cm^3). Approximately 10 μL of the solution was extricated from the syringe to maintain a stationary hanging drop on the tip of the needle, fully submersing the thermocouple bead inside the sample drop. A piece of graph paper was placed near the drop to provide scale (see figure 1). The laser

was aligned to pass through the drop without hitting the thermocouple. The chopper was turned on. The data collection was initiated on the datalogger, the record button was pressed on the DVD recorder, and the laser shutter was then opened. As the laser irradiated the sample, the temperature began to increase. Data was collected until equilibrium temperature was reached. After reaching equilibrium, the laser shutter was closed and the return to ambient temperature was logged. As the voltage vs. time data was collected, the camera and DVD recorder simultaneously captured video of the laser passing through the drop. The software program Image J was used to determine the width and height of the drop. Using the equation of an ellipsoid, the volume of the drop was approximately determined. The pathlength of the laser through the drop was also determined from the captured video.

Results

The temperature trace of a 7×10^{10} particles/cm^3 solution of 20 nm colloidal gold nanoparticle solution drawn out in a droplet and excited with 0.28 W CW laser excitation at 532 nm is shown in figure 2. The droplet temperature reached steady state after ~ 60 s of excitation. The laser shutter was activated at this point and the decay back to the ambient temperature was followed. The inset in figure 2 shows a natural log plot of $\frac{T(t) - T_o}{T_{\max} - T_o}$ as a function of time right after the laser was turned off. The linear relationship shows that a first order decay is observed for the temperature decay back to the ambient temperature. The blue dash line in the figure is the fit of the data using the decay constant from the inset. The red dash line in the figure is our model fit to the data (see discussion section). The inset in the upper left hand corner of the figure is the residual of the data compared to our model fit. The temperature limits in the inset is ± 1 °C. The root-mean-squared (rms) deviation of our model compared to the data shows an uncertainty in the model fit of 0.44 °C.

The temperature trace of the same droplet with different laser intensities was collected and shown in figure 3. Again, the red dash line is the fit of our model to the data. The intensity of the laser is 0.28 W, 0.23 W and 0.14 W. The temperature maximum in the droplet scaled with laser intensity.

The laser intensity was modulated with a chopper set before the excitation of the droplet. The temperature trace of a droplet with chopped laser intensity is shown in figure 4. An anisotropic square-wave waveform was applied to the laser intensity as shown in the inset in figure 4. The laser intensity before chopping was 0.28 W. The laser was on for 2 ms out of 5 ms resulting in a 60% reduction in the overall laser intensity. The fit of our model to the data is shown as the red dash line and the difference in the model fit to the data is shown in the upper inset. The temperature limits in the inset is ± 1 °C.

Discussion

Model. Energy balance equation

Our macroscopic model is similar to the ones previously published.[53, 54] It starts with the energy balance equation (equation 1) where energy is supplied by absorption of the gold colloidal solution by the laser light (Q_I) and dissipated by transfer to an external reservoir (Q_{ext}).

$$\sum_i m_i C_{p,i} \frac{dT}{dt} = Q_I - Q_{ext} \quad (1)$$

In this equation $m_iC_{p,i}$ are the mass and heat capacity components of the system, T is the temperature, and t is time. The rate of energy supplied to the system is given in equation 2 where I is the incident laser power, A_λ is the absorbance of the nanoparticle solution and η is the efficiency of converting light absorption to thermal energy.

$$Q_I = I(1 - 10^{-A_\lambda})\eta \tag{2}$$

Here $A_\lambda = l_{opt} \cdot C \cdot \varepsilon$, where l_{opt}, C, and ε are the optical path, molar concentration, and molar extinction coefficient respectively. For the experimental situation shown in Fig. 1, $l_{opt} = 0.186$ cm, C=1.24*10^{-10} mol/L, n_{NP}=7.49 · 10^{10} cm^{-3}, and ε=9.38 · 10^8 $M^{-1}cm^{-1}$. This molar extinction coefficient corresponds to the particle cross section (σ_{par}) of $\sigma_{par} = \varepsilon \bullet \frac{10^8}{N_A} = 1.56 \bullet 10^{-12} \mathrm{cm}^2/particle$. This is the typical number found in the literature. The resulting absorbance (A_λ) is 0.0217.

The rate of energy flowing out of the system is given by equation 3 where the dissipation energy is assumed to be proportional to a linear thermal driving force that has a heat transfer coefficient, h, and S is the cross sectional area perpendicular to conduction.

$$Q_{ext} = hS(T - T_o) \tag{3}$$

Equation 1 can be recast into a simpler form (equation 4) by collecting terms and a variable change, T^*, where $T^*$is the temperature difference ($T - T_o$) from the ambient temperature T_o.

$$\frac{dT^*}{dt} = A - BT^* \tag{4}$$

A and B are given in equations 5 and 6 respectively where A(°C/s) is the rate of energy absorption and B(s^{-1}) the rate constant associated with heat loss. The mass (m_w) and heat capacity ($C_{p,w}$) components of the system have been limited to just the dominant component of water forming the droplet.

$$A = \frac{Q_I}{\sum_i m_i C_{p,i}} = \frac{I(1 - 10^{-A_\lambda})\eta}{m_w c_{p,w}} \tag{5}$$

$$B = \frac{hS}{m_w C_{p,w}} \tag{6}$$

The rate constant of heat loss from the droplet to an external reservoir (B) is determined by following the temperature decay back to the ambient temperature after the laser excitation is turned off. In this regime, the temperature trace is given by equation 7,

$$T(t)=T_o+(T_{\max}-T_o)\exp(-Bt) \text{ when A=0,} \tag{7}$$

where T_{max} is the temperature when the laser is blocked. Equation 8 gives the steady-state temperature (T_{ss}) during laser excitation. The steady -state temperature inside the droplet is assumed to be uniform and unchanging in the droplet and is achieved when the rate of energy absorption is equal to the rate of heat loss. The efficiency of converting absorbed light to heat (η) is extracted from the experimental curves by solving equation 9 where

$\Delta T=T(t\to\infty)-T_o=\frac{A}{B}$ and m_w, V_w, and c_w are the mass and volume of the droplet, and the specific heat capacity of water, respectively. The saturation temperature measured in the experiment in Fig. 2 is in the interval 28.75 °C<ΔT_{ss}<29. 25 °C. With the measured droplet volume of 0.0035 cm^3, B=0.120 s^{-1}, and I=0.28W, we obtain: 0.97<η<1.03. The calculated η is remarkably close to 1, as expected for small NPs. For larger NPs, we expect η to become essentially smaller than 1 due to the scattering effect. The parameter η is obtained from the following equations.

$$\frac{dT^*}{dt}=0, \text{ then } \Delta T=T_{ss}-T_o=\frac{A}{B}=\frac{I(1-10^{-A_\lambda})\eta}{B\sum_i m_i C_{p,i}} \tag{8}$$

$$\eta=\frac{B(T_{ss}-T_o)\rho_w c_w V_w}{I(1-10^{-A_\lambda})} \tag{9}$$

Finally, the temperature profile after the laser is turned on is given by equation 10.

$$T(t)=T_o+\frac{A}{B}(1-\exp(-Bt)) \text{ when A}\neq 0 \tag{10}$$

Model fit to the data

The rate of heat loss, B, was determined by plotting $\ln\frac{T-T_o}{T_{\max}-T_o}$ versus time. The resultant plot was nearly linear with the slope equal to B, the rate constant for heat loss. Such a plot is shown in the inset in figure 2 where B is determined to be 0.120 s^{-1}. The blue dash line in figure 2 is our modeled fit to the data using B for the rate constant. The rate of energy absorption is determined by measuring the absorption of light at 532 nm for the droplet solution in a 1 cm quartz cuvette. The path length through the droplet was measured by capturing a picture of the droplet during excitation and directly measuring the distance the light travelled. Once the path length is known then the amount of absorption is determined by scaling the absorbance from the solution in the cuvette to the path length through the droplet. This absorption is used with the laser power, the heat capacity of water, and the mass of the droplet to determine the rate of energy absorption (see equation 5). The mass of the droplet was determined by determining the volume of the droplet using the picture taken during excitation. The droplet size and laser path length were determined by analyzing the image of the droplet with image J. A scale was set next to the droplet for an absolute reference of distance (see figure 1). Once the volume of the droplet was known then the mass was ascertained using the density of water. The mass and

heat capacity of the thermocouple and needle were relatively insignificant compared to the mass and heat capacity of the droplet. Thus, only the droplet mass and heat capacity were considered in our model.

The red-dashed line in figure 2 shows our modeled fit to the data with CW laser excitation. There are no adjustable parameters in the fit. The efficiency of converting light absorption into heat, η, is 1 ±0.03. The difference between the model and data is shown in the upper inset. The temperature scale is ±1 °C. The rms deviation of the model to the data was calculated over the entire time interval shown in the upper inset and is equal to 0.40 °C. The rms deviation for our baseline temperature is 0.14 °C. Most of the discrepancy in our model to the data is observed at the initial rise in temperature but this discrepancy is reduced considerably when lower laser power was used with a subsequent lower temperature differences (see figures 3 and 4). Our fit is very sensitive to the size of the droplet with relatively minor changes in size resulting in a large difference in the fit. For this reason care was taken to determine an accurate value for the size of the droplet during laser excitation.

The droplet temperature trace for CW excitation with different laser powers is shown in figure 3. The red-dashed line is the model fit to the data using the rate constant for heat loss, laser power, and droplet size for each trace. In all cases, the temperature profile during laser excitation to the steady-state temperature can be modeled with a conversion efficiency, η, equal to unity. The rate constant for heat loss varied from 0.106 s^{-1} to 0.110 s^{-1}.

We tested the effect that laser modulation has upon η by chopping the laser with a waveform shown in the inset in figure 4. This particular waveform reduced the laser power by 60%(The laser was on for 2 ms out of 5 ms). The red-dashed line in the figure is the model fit using the starting laser power of 0.28 W attenuated by 60% to 0.112 W, a heat loss rate of 0.119 s^{-1} and the corresponding droplet size. The difference in the model fit to the data is shown in the upper inset. The temperature scale is ± 1 °C and the rms deviation in the modeled fit is 0.19 °C which is close to the baseline rms deviation in temperature of 0.14 °C.

Comparison of a suspension of colloidal NPs to a single particle

We now model a temperature distribution is an optically-simulated water droplet. First of all, we have to consider mechanisms of heat release from the droplet. The heat release can come from thermal transfer through (a) water-air interface via convection and (b) through metallic wires and syringe needle. To understand the mechanism, we performed another experiment: a NP-water droplet was submerged into a hydrophobic liquid (perfluoradecalin) that has low heat conductivity to suppress the heat loss at the water-air interface. We did not see significant reduction of cooling and can conclude that the most probable mechanism of cooling is heat release from the droplet via the metallic syringe needle (the cross section of syringe is larger than the cross sectional area of thermo couple wires). We tested this assumption by substituting a glass pipet for the metallic needle resulting in a decrease in the heat loss constant by a factor of ~2. Another important assumption of the above formalism is a rapid temperature equilibration within the water droplet so that the whole droplet is described by the same temperature $T(t)$at any time instant t. The characteristic time to establish thermal equilibrium in a droplet heated non-uniformly by a laser beam (see Fig. 1) is $\Delta t_{diff} \sim \frac{L^2}{D_w}$, where $L$and D_w are a size and thermal diffusivity of water, respectively. With $L \sim 0.1\ cm$ and $D_w = 1.4 \cdot 10^{-3}$ cm^2/s, we obtain $\Delta t_{diff} \sim 7s$. This is comparable with the observed $B^{-1} = 8.3$ s. However, we think that the dominant mechanism of temperature equilibration in the droplet is convection of water. To prove this, we put a small number of glass beads in the droplet and imaged the motion of the beads. Interestingly, we observed very active motion of the beads before laser excitation and after laser excitation in the steady state when the temperature becomes saturated

at its maximum and should be uniform in the droplet. The speed of motion of beads was about *1 mm/s* and, therefore, the temperature equilibration due to the convectional flow in the mm-size droplet should happen within one or, at least, few seconds. The students were not surprised a bit, but we were. From this we concluded that the most probable mechanism of temperature equilibration in the droplet is the convectional flow and mixing of liquid that happens at the time scale shorter than B^{-1} and Δt_{diff}. Another argument towards the fast temperature equilibration in the droplet is that the simple single exponential function for the temperature dynamics (eqs. 7–8) provides an excellent description for the experimental observations (Fig. 2). We plan on another paper describing the convectional flow induced by light heating. For a convectional motion of fluid with suspended gold NPs, a modeling becomes very challenging and represents a computational task. The set of equations includes the nonlinear Navier-Stokes equation and the thermal transfer equation[55]. The latter is:

$$\frac{\partial \rho(\mathbf{r},t)\, c(\mathbf{r},t)\Delta T\,(\mathbf{r},t)}{\partial t}+\mathbf{v}(\mathbf{r},t)\cdot\frac{\partial \rho(\mathbf{r},t)\, c(\mathbf{r},t)\Delta T\,(\mathbf{r},t)}{\partial \mathbf{r}}=\nabla k(\mathbf{r},t)\nabla\Delta T(\mathbf{r},t)+q(\mathbf{r},t), \tag{11}$$

where $T(\mathbf{r},t)$ is temperature as a function of coordinate $\mathbf{r}$ and time t, $\rho(\mathbf{r},t)$, $c(\mathbf{r},t)$ and $k(\mathbf{r},t)$are the mass density, specific heat, and thermal conductivity, respectively; $\mathbf{v}(\mathbf{r},t)$ is the local velocity of medium. These parameters depend on time and coordinate because we deal with moving gold NPs in water. The local heating $q(\mathbf{r},t)$comes from energy dissipation by Au NPs [52],

$$q(\mathbf{r},t)=\langle \mathbf{j}(\mathbf{r},t)\cdot\mathbf{E}(\mathbf{r},t)\rangle_t=-\frac{1}{2}\mathrm{Re}\left[i\omega\frac{\varepsilon(\mathbf{r},t)-1}{4\pi}\,\tilde{\mathbf{E}}\,(\mathbf{r})\tilde{\mathbf{E}}^{*}(\mathbf{r})\right], \tag{12}$$

where $\mathbf{j}(\mathbf{r},t)$ is the current density, $\mathbf{E}(\mathbf{r},t) = \mathrm{Re}[\tilde{\mathbf{E}}(\mathbf{r})\cdot e^{-i\omega t}]$ is the resulting electric field in the system, and $\varepsilon(\mathbf{r},t)$is the local dielectric constant of the medium. The function $q(\mathbf{r},t)$ describes the heat generation inside the droplet from moving heat sources i.e., optically-excited NPs. Here we assume that the system is excited with an external laser field $\mathbf{E}_0(t) = \mathrm{Re}[\tilde{\mathbf{E}}_0(t)\cdot e^{-i\omega t}]$ and that $\varepsilon(\mathbf{r},t) = \varepsilon_m$ inside the Au NPs and $\varepsilon(\mathbf{r},t) = \varepsilon_0$ elsewhere. The dielectric constants of metal and matrix are ε_m and ε_0 respectively. The corresponding light flux is $i_0=c\mathbf{E}_0^{\,2}\sqrt{\varepsilon_0}/8\pi$. Here and later we assume that the density of NPs is small and overall electromagnetic properties of the NP-water solution are not much affected by NPs. For example, for our experimental conditions, the absorbance from the droplet containing colloidal NPs is only about 2%.

In our system, NPs are moving in convectional flow together with water. A characteristic size of such a flow is about the size of our droplet, *L~1mm*. Therefore, the NP size is much smaller than the flow size. If such, we can consider a small part of our droplet and assume that the flow velocity is uniform within this part. Then, we can eliminate the second, kinematic term in the left-hand side of eq. 11 by introducing a new variable: $\mathbf{r}' = \mathbf{r} - \mathbf{v}\cdot t$. In the new moving frame, we obtain

$$\frac{\partial \rho(\mathbf{r})\, c(\mathbf{r})\Delta T(\mathbf{r}',t)}{\partial t}=\nabla k(\mathbf{r})\nabla T(\mathbf{r}',t)+q(\mathbf{r}'). \tag{13}$$

Our NP solution is very diluted with an average distance between NPs of $l_{NP}=\frac{1}{\sqrt[3]{\eta_{NP}}}=2370\,\text{nm} \gg d_{NP}=20\,\text{nm}$, where d_{NP} is the NP diameter and $\eta_{NP} = 7.49 \cdot 10^{10}$ cm^{-3} is the particle density. Since $l_{NP} \gg d_{NP}$, we can focus on a single NP that is caught up in water currents that enter the region of laser excitation. We observe, using glass beads, that the flow of NPs cross the laser beam in fractions of a second. When a single NP crosses the beam it absorbs light energy and start releasing heat. A characteristic time to establish the temperature profile around a single NP at distances ~d_{NP} is about: $\Delta t \sim \frac{d_{NP}^2}{2D_w}$ [52]. This gives a rather short time: 1.4 ns. Therefore, we can conclude that, in a flow, a single NP establishes the temperature distribution around itself rather fast. The steady-state solution of the equation is well known[52]:

$$T(\mathbf{r})=T_{av}+\frac{V_{NP}}{4\pi k_w}\frac{q_0}{r};\ (r>R_{NP}), \tag{14}$$

where k_w is the thermal conductivity of water, r is the distance from the NP surface, R_{NP} and V_{NP} are the NP radius and volume, respectively; q_0 is rate of heat generation within a single NP. Importantly, the temperature T_{av} is created by all other NPs in the vicinity of the NP of interest. The maximum temperature increase occurs, of course, at the NP surface: $\Delta T_{\max}=T_{\max}-T_{av}=\frac{V_{NP}}{4\pi k_w}\frac{q_0}{R_{NP}}$. We now estimate $\Delta T_{\max}$ for the parameters of the experiment. From eqs. 12 and 14, we have:

$$\Delta T_{\max}(i_0)=\frac{R_{NP}^2}{3k_0}\text{Re}\left[i\omega\frac{1-\varepsilon(\mathbf{r})}{8\pi}\left|\frac{3\varepsilon_0}{2\varepsilon_0+\varepsilon_m}\right|^2\right]\frac{8\pi\cdot i_o}{c\sqrt{\varepsilon_0}} \tag{15}$$

Using the optical dialectic constant of Au taken from the tables[56] and taking the water constant (ε_0 =1.8), we have an estimate: $\Delta T_{\max} = 2.2 \cdot 10^{-2}\ ^\circ C$ for $i_o = P/A_{laser} = 400\ W/cm^2$ and for the wavelength of the plasmon peak; here the laser power $I = 0.28\ W$ and the laser beam cross section $A_{laser} = 0.07 mm^2$. The calculated local temperature increase corresponds to the theoretical molar extinction coefficient of $\varepsilon_{\text{theory}}=1.0*10^9\ \text{M}^{-1}\text{cm}^{-1}$; this number is close to the experimental value. We can see that the local increase of temperature at the surface of a single NP is really very small. The overall increase of temperature in the system originates from release of energy from many optically-stimulated NPs. In other words, we deal here with a collective heating effect. Assuming rapid mixing and temperature equilibration inside a droplet, the average temperature increase becomes

$$\Delta T=T_{av}-T_o=\eta\frac{I(1-10^{-A_\lambda})}{B\rho_w c_w V_w}\approx 2.303\frac{\eta l_{opt}\varepsilon CI}{B\rho_w c_w V_w}, \tag{16}$$

where the heat release constant B depends on the thermal contact of the droplet and the external world. Taking measured $\eta = 1$ and $B = 0.120\ s^{-1}$, we reproduce the observed temperature increase of $\Delta T \sim 8\ ^\circ C$ (see Fig. 2). The important property of eq. 16 is that $\Delta T \propto C$, i.e. a measurable increase in temperature is generated by many NPs whereas a single NP does not create a temperature increase even on its surface.

We now demonstrate the effect of heat accumulation for a simplified model system. First, we neglect convection. Second, we assume that the system has uniform background heat conductivity, i.e. the system is open. In our experiment, we also deal with an open system since heat is realized to the surroundings relatively fast. The details of heat release at the droplet interface are important for a quantitative description of the data. A simplified model system with uniform background heat conductivity corresponds to a typical situation occurring in bio-medical applications of hot NPs: i.e., NPs are injected into a small cavity inside a massive tissue and become optically stimulated. Tissue typically has the heat conductivity of water and heat from hot NPs is likely to flow isotropically inside the tissue. We now solve eq. 13 on the macroscale under stationary conditions for static NPs and with our simplifying assumptions. As we have shown, at the nanoscale, the temperature does not change much if the laser flux is relatively low. [52] The heat source, $q(\mathbf{r})$, can be modeled using an averaged density of NPs, η_{NP}, and position-dependent light intensity $i(\mathbf{r})$. Heated NPs form a cylinder with dimensions of laser beam (see Figure 5). Then, we have $q(\mathbf{r}) = \eta_{NP}\alpha_o i(\mathbf{r})$ where

$\alpha_o = -V_{NP}\mathrm{Re}[\frac{i\omega(\varepsilon_m - 1)}{c\sqrt{\varepsilon_o}}|\frac{3\varepsilon_o}{2\varepsilon_o+\varepsilon_m}|]^2$. The solution of eq. 13 is equivalent to a solution of Poisson equation from electrostatics:

$$\Delta T(\mathbf{r}) = \frac{i_o \alpha_o n_{NP}}{4\pi k_w}\int_{beam}\frac{dV'}{|\mathbf{r}-\mathbf{r}'|} = \Delta T_{\max} R_{NP}\eta_{NP}\int_{beam}\frac{dV'}{|\mathbf{r}-\mathbf{r}'|} \quad (17)$$

here the integral should be taken over a cylindrical volume of beam and $i_o = \frac{I}{A_{beam}}$ is the light flux inside the beam (see Fig. 5a). NPs are assumed to be distributed uniformly in space. For an elongated cylindrical beam we can estimate the eq. 17:

$\Delta T(r=0) \approx \Delta T_{\max} R_{NP}\eta_{NP}A_{beam}2Ln[\frac{l_{opt}}{R_{beam}}] = 5.8^{\circ}C$. We took the NP density, light intensity, optical path and other parameters similar to those in the experiment. We can see that, for a submerged NP cylinder (Fig. 5a), we obtain a realistic peak temperature which is not very far from the observed one for a photo-stimulated droplet in air (Fig. 5b). However, a calculated temperature averaged over a distance of about 1 mm is less than that observed in the droplet experiment (Fig. 5b); this is due to fast removal of heat in the open system modeled by us. The graphs and insets in Figs. 5b and 5c represent both a macroscopic and nanoscopic picture. On the nanoscale, the temperature profile within the hot cylinder area has small "bumps" in temperature due to single optically-stimulated NPs (Fig. 5b). A size of a "bump" was estimated as a local increase of temperature at the surface of a single NP: $\Delta T_{\max} = 2.2 \cdot 10^{-2}\,^{\circ}C$. A sizable overall increase of temperature in the system is due to a collective heating effect of many NPs, $V_{beam}\eta_{NP} \sim 10^7$. If, on the other hand, the solution of NPs in the droplet is diluted ($n_{NP} = 7.49 \cdot 10^6\ cm^{-3}$) and excited with a larger laser flux ($i_o = 5 \cdot 10^4\ W/cm^2$) the temperature variations observed above is reversed. Now (see Figure 5c) the change in the local averaged temperature is small (~0.1 °C) with a much larger increase in the temperature variation around the single NPs (~3 °C).

Conclusion

We measured the temperature change in a water droplet containing a colloidal suspension of 20 nm Au NPs after CW laser excitation at 532 nm. The Au NPs absorb ~2% of the light and convert the absorbed energy into heat with a transduction efficiency of η. The steady-state temperature measured is in the interval 28.75 °C<ΔT<29.25 °C. Using the measured droplet volume of 0.0035 cm^3, the rate constant for heat dissipation from the droplet (B) of 0.120 s^{-1}, and the laser power (I) of 0.28W, we obtain the transduction efficiency within the interval

of 0.97<η<1.03. The calculated η is remarkably close to 1, as expected for small NPs and is invariant to laser modulation. We then modeled the temperature distribution inside the optically-stimulated water droplet and found that, on the nanoscale, the temperature profile within the hot cylinder area has small "bumps" in temperature located around single optically-stimulated NPs. The size of a "temperature bump" was estimated to be $\Delta T_{\max} = 2.2 \cdot 10^{-2}$ °C for the conditions of our experiment. A sizable overall increase in the temperature of the droplet is observed due to a collective heating effect of many NPs within the excitation volume, $V_{beam}\eta_{NP} \sim 10^7$. If, on the other hand, the particle density is reduced ($n_{NP} = 7.49 \cdot 10^6\ cm^{-3}$) and larger laser flux is used ($i_o = 5 \cdot 10^4\ W/cm^2$) large temperature spikes around the NPs is observed (~3 °C) with little change in the ambient temperature (~0.1 °C).

Acknowledgements

We should acknowledged BNNT, NIH and NSF.

References

1. Qian XM, Nie SM. Chemical Society Reviews 2008;37(5):912–920. [PubMed: 18443676]
2. Murray CB, Kagan CR, Bawendi MG. Annual Review Of Materials Science 2000;30:545–610.
3. Hartland GV. Annual Review Of Physical Chemistry 2006;57:403–430.
4. Eustis S, El-Sayed MA. Chemical Society Reviews 2006;35(3):209–217. [PubMed: 16505915]
5. Nehl CL, Hafner JH. Journal Of Materials Chemistry 2008;18(21):2415–2419.
6. Schwartzberg AM, Zhang JZ. Journal Of Physical Chemistry C 2008;112(28):10323–10337.
7. Noguez C. Journal Of Physical Chemistry C 2007;111(10):3806–3819.
8. Plech A, Kotaidis V, Gresillon S, Dahmen C, von Plessen G. Physical Review B 2004;70(19):195423.
9. Hu M, Wang X, Hartland GV, Salgueirino-Maceira V, Liz-Marzan LM. Chemical Physics Letters 2003;372(5–6):767–772.
10. Richardson HH, Hickman ZN, Govorov AO, Thomas AC, Zhang W, Kordesch ME. Nano Letters 2006;6(4):783–788. [PubMed: 16608284]
11. Huang W, El-Sayed MA. European Physical Journal-Special Topics 2008;153:325–333.
12. Petrova H, Hu M, Hartland GV. Zeitschrift Fur Physikalische Chemie-International. Journal Of Research In Physical Chemistry & Chemical Physics 2007;221(3):361–376.
13. Huang XH, El-Sayed IH, Qian W, El-Sayed MA. Journal Of The American Chemical Society 2006;128(6):2115–2120. [PubMed: 16464114]
14. Yao CP, Zhang ZX, Yao BL. Progress In Biochemistry And Biophysics 2007;34(3):312–316.
15. Govorov AO, Richardson HH. Nano Today 2007;2(1):30–38.
16. Huang XH, Jain PK, El-Sayed IH, El-Sayed MA. Photochemistry And Photobiology 2006;82(2): 412–417. [PubMed: 16613493]
17. Khlebtsov B, Zharov V, Melnikov A, Tuchin V, Khlebtsov N. Nanotechnology 2006;17(20):5167–5179.
18. Takahashi H, Niidome T, Nariai A, Niidome Y, Yamada S. Nanotechnology 2006;17(17):4431–4435.
19. Hu M, Petrova H, Chen JY, McLellan JM, Siekkinen AR, Marquez M, Li XD, Xia YN, Hartland GV. Journal Of Physical Chemistry B 2006;110(4):1520–1524.
20. Liu GL, Kim J, Lu Y, Lee LP. Nature Materials 2006;5(1):27–32.
21. Zharov VP, Mercer KE, Galitovskaya EN, Smeltzer MS. Biophysical Journal 2006;90(2):619–627. [PubMed: 16239330]
22. Huang WY, Qian W, El-Sayed MA. Journal Of Applied Physics 2005;98(11):114301.
23. Mercuri F, Zammit U, Scudieri F, Marinelli M. Journal De Physique Iv 2005;125:135–139.
24. Link S, El-Sayed MA. International Reviews In Physical Chemistry 2000;19(3):409–453.
25. Reismann M, Bretschneider JC, von Plessen G, Simon U. Small 2008;4(5):607–610. [PubMed: 18454511]

26. Durr NJ, Larson T, Smith DK, Korgel BA, Sokolov K, Ben-Yakar A. Nano Letters 2007;7(4):941–945. [PubMed: 17335272]
27. Gobin AM, O'Neal DP, Watkins DM, Halas NJ, Drezek RA, West JL. Lasers In Surgery And Medicine 2005;37(2):123–129. [PubMed: 16047329]
28. Visaria R, Bischof JC, Loren M, Williams B, Ebbini E, Paciotti G, Griffin R. International Journal Of Hyperthermia 2007;23(6):501–511. [PubMed: 17952764]
29. Visaria RK, Griffin RJ, Williams BW, Ebbini ES, Paciotti GF, Song CW, Bischof JC. Molecular Cancer Therapeutics 2006;5(4):1014–1020. [PubMed: 16648573]
30. El-Sayed IH, Huang XH, El-Sayed MA. Cancer Letters 2006;239(1):129–135. [PubMed: 16198049]
31. Lapotko DO. Lasers In Surgery And Medicine 2006;38(3):240–248. [PubMed: 16470847]
32. Lapotko DO, Lukianova E, Oraevsky AA. Lasers In Surgery And Medicine 2006;38(6):631–642. [PubMed: 16736503]
33. Chen JY, Wang DL, Xi JF, Au L, Siekkinen A, Warsen A, Li ZY, Zhang H, Xia YN, Li XD. Nano Letters 2007;7(5):1318–1322. [PubMed: 17430005]
34. Gobin AM, Lee MH, Halas NJ, James WD, Drezek RA, West JL. Nano Letters 2007;7(7):1929–1934. [PubMed: 17550297]
35. Stehr J, Hrelescu C, Sperling RA, Raschke G, Wunderlich M, Nichtl A, Heindl D, Kurzinger K, Parak WJ, Klar TA, Feldmann J. Nano Letters 2008;8(2):619–623. [PubMed: 18220441]
36. Jain PK, Qian W, El-Sayed MA. Journal Of The American Chemical Society 2006;128(7):2426–2433. [PubMed: 16478198]
37. Slocik JM, Tam F, Halas NJ, Naik RR. Nano Letters 2007;7(4):1054–1058. [PubMed: 17378619]
38. Zharov VP, Lapotko DO. Ieee Journal Of Selected Topics In Quantum Electronics 2005;11(4):733–751.
39. Loo C, Lowery A, Halas N, West J, Drezek R. Nano Letters 2005;5(4):709–711. [PubMed: 15826113]
40. Loo C, Lin A, Hirsch L, Lee MH, Barton J, Halas N, West J, Drezek R. Technology In Cancer Research & Treatment 2004;3(1):33–40. [PubMed: 14750891]
41. Cognet L, Tardin C, Boyer D, Choquet D, Tamarat P, Lounis B. Proceedings Of The National Academy Of Sciences Of The United States Of America 2003;100(20):11350–11355. [PubMed: 13679586]
42. Boyer D, Cognet L, Tamarat P, Maali A, Choquet D, Orrit M, Lounis B. Biophysical Journal 2003;84(2):24A–24A.
43. Sokolov K, Follen M, Aaron J, Pavlova I, Malpica A, Lotan R, Richards-Kortum R. Cancer Research 2003;63(9):1999–2004. [PubMed: 12727808]
44. Paciotti GF, Kingston DGI, Tamarkin L. Drug Development Research 2006;67(1):47–54.
45. Paasonen L, Laaksonen T, Johans C, Yliperttula M, Kontturi K, Urth A. Journal Of Controlled Release 2007;122(1):86–93. [PubMed: 17628159]
46. Otsuka H, Nagasaki Y, Kataoka K. Advanced Drug Delivery Reviews 2003;55(3):403–419. [PubMed: 12628324]
47. Jain PK, Huang X, El-Sayed IH, El-Sayad MA. Plasmonics 2007;2(3):107–118.
48. Everts M, Saini V, Leddon JL, Kok RJ, Stoff-Khalili M, Preuss MA, Millican CL, Perkins G, Brown JM, Bagaria H, Nikles DE, Johnson DT, Zharov VP, Curiel DT. Nano Letters 2006;6(4):587–591. [PubMed: 16608249]
49. Richardson HH, Thomas AC, Carlson MT, Kordesch ME, Govorov AO. Journal Of Electronic Materials 2007;36(12):1587–1593.
50. Hartland GV, Hu M, Sader JE. Journal Of Physical Chemistry B 2003;107(30):7472–7478.
51. Dulkeith E, Niedereichholz T, Klar TA, Feldmann J, von Plessen G, Gittins DI, Mayya KS, Caruso F. Physical Review B 2004;70(20):205424.
52. Govorov AO, Zhang W, Skeini T, Richardson H, Lee J, Kotov NA. Nanoscale Research Letters 2006;1(1):84–90.
53. Roper DK, Ahn W, Hoepfner M. Journal Of Physical Chemistry C 2007;111(9):3636–3641.
54. Kim DK, Amin MS, Elborai S, Lee SH, Koseoglu Y, Muhammed M, Muhammed M. Journal Of Applied Physics 2005;97(10):10J510.

55. Landau, LD.; Lifschitz, EM. Fluid Mechanics (Course of Theoretical Physics). Vol. 2. Vol. 6. Pergamon Press; 1987.

56. Palik, ED. Handbook of Optical Constants of Solids. Academic Press; New York: 1985.

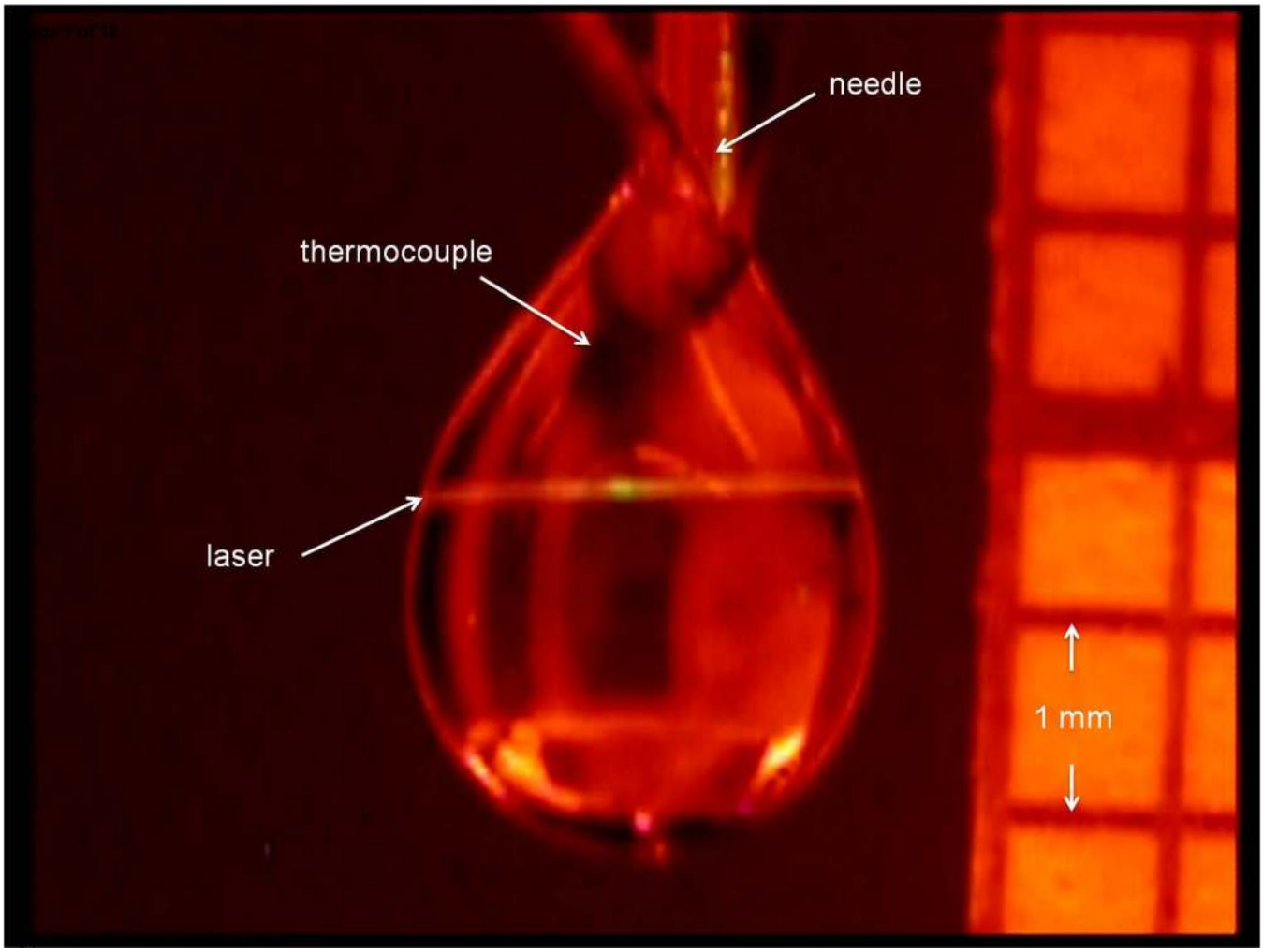

Figure 1.
Image of typical water droplet taken during laser excitation. The thermocouple (highlighted in the image) is embedded in the droplet. The droplet is located at the end of a stainless steel needle. The size (volume) of the droplet is determined by comparison of a grid positioned next to the droplet.

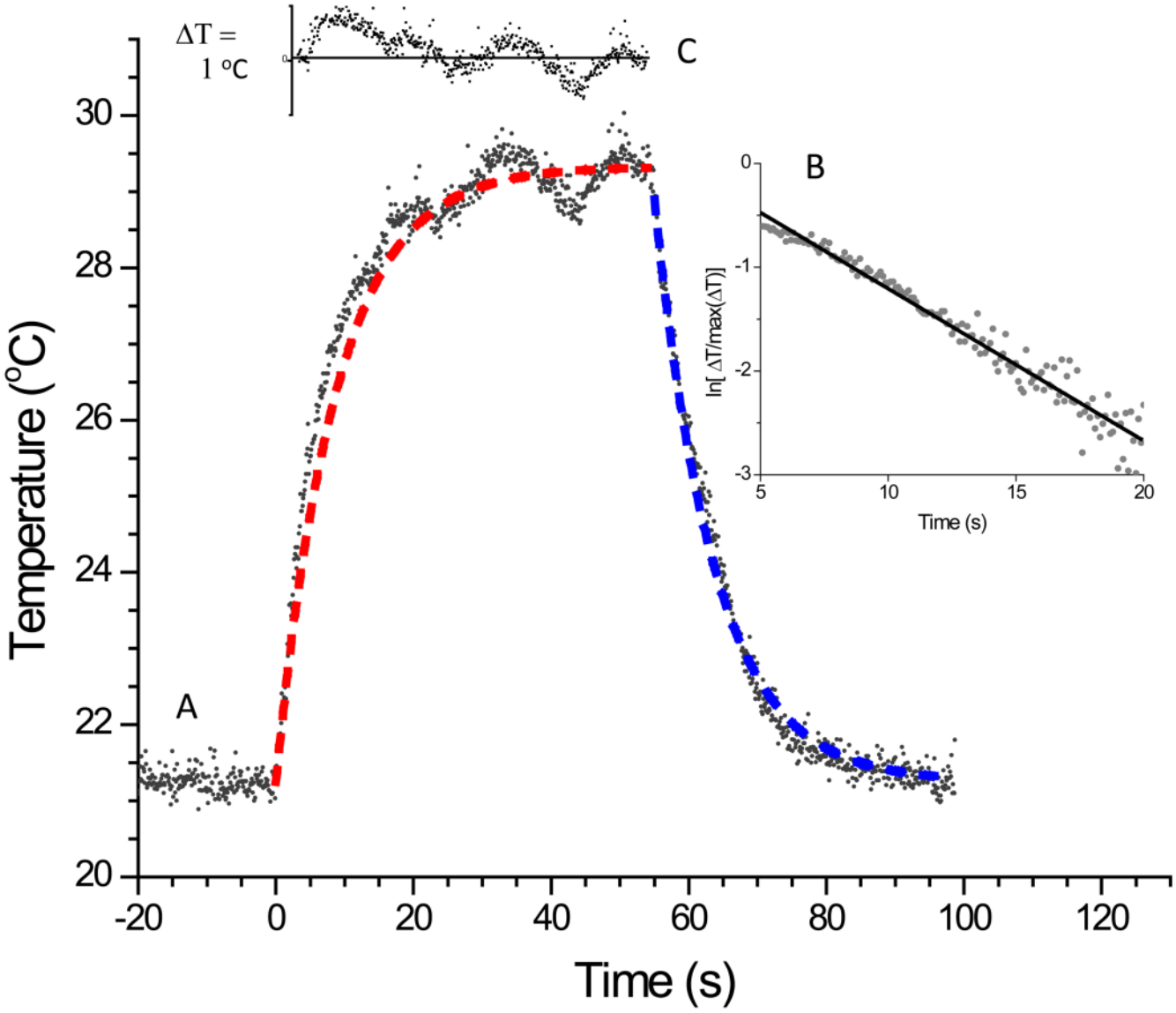

Figure 2.

(A) Typical temperature trace showing increase in temperature after laser excitation (time = 0) and temperature decay back to the ambient after the laser is shut off (~time = 60 seconds).

(B) Plot of the natural log of $\frac{T(t) - T_o}{T_{\max} - T_o}$ as a function of time right after the laser was turned off. The linear relationship shows that a first order decay is observed for the temperature decay back to the ambient temperature. The blue dash line in the figure is the fit of the data using the decay constant obtained from this plot. The red dash line in the figure is our model fit to the data with η equal to 1. (C) Plot of the residual of the data compared to our model fit.

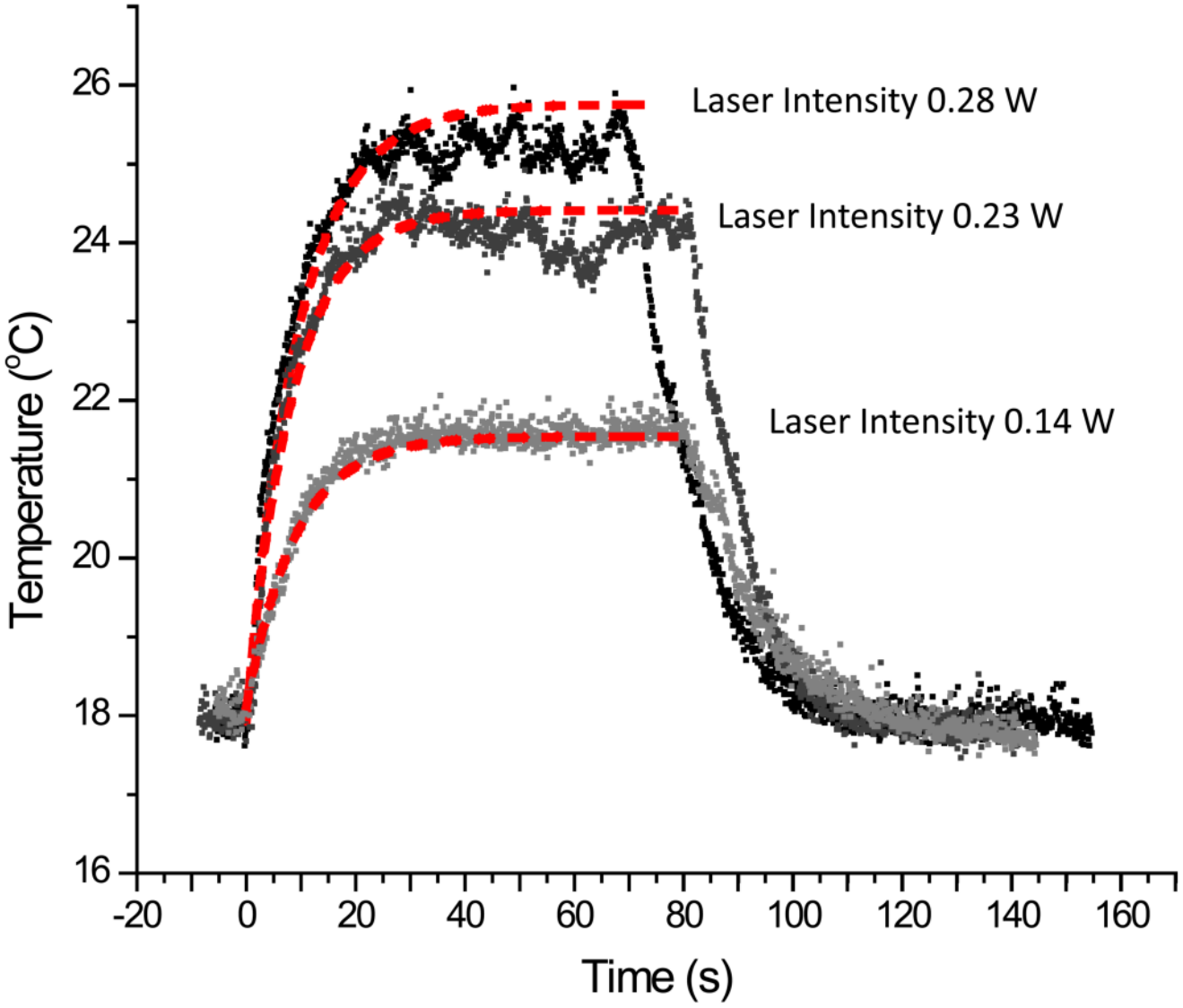

Figure 3.
The temperature trace of the same droplet with different laser intensities. The red dash line is the fit of our model to the data with η equal to 1. The intensity of the laser is 0.28 W, 0.23 W and 0.14 W.

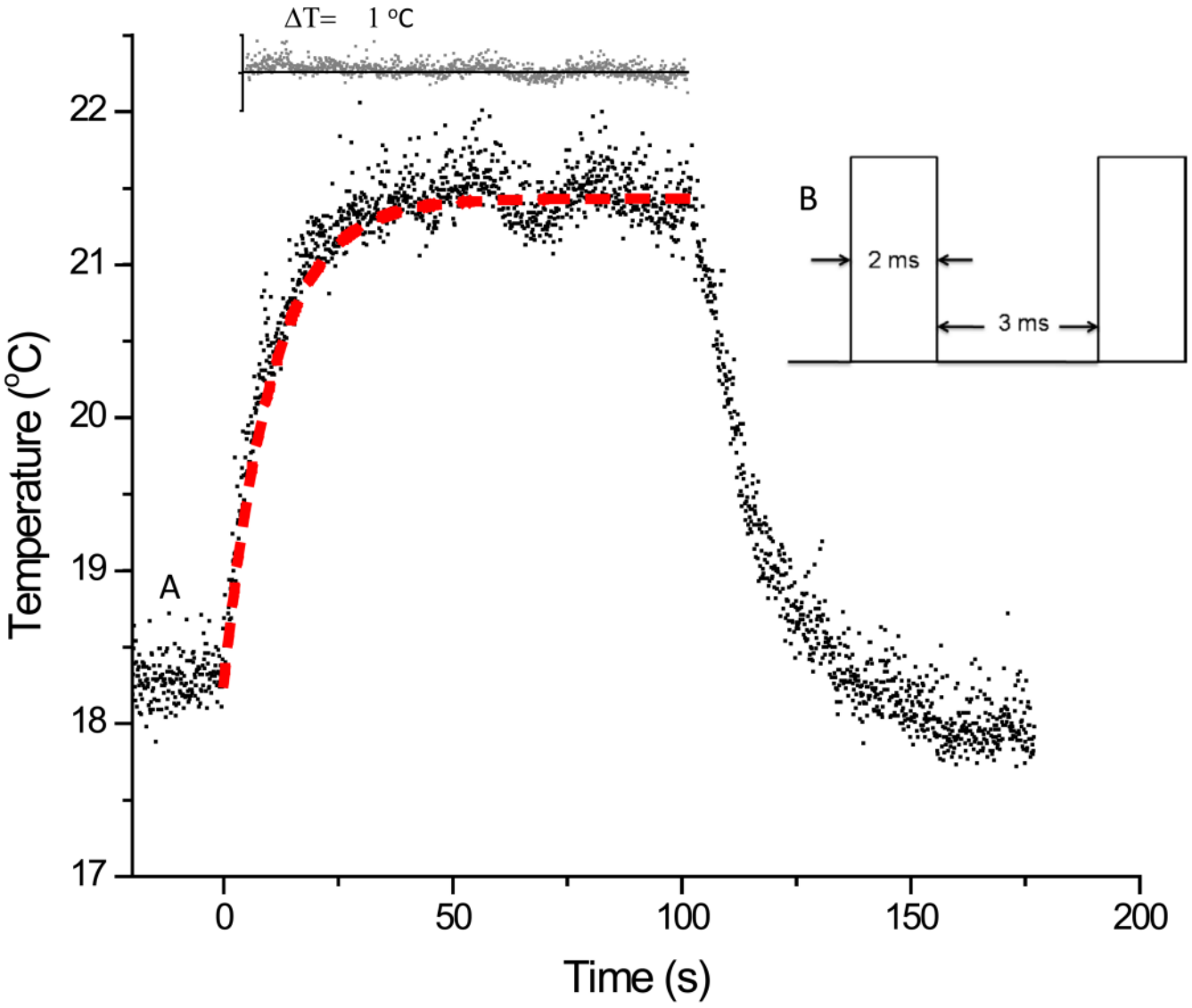

Figure 4.

(A) The temperature trace of a droplet with chopped laser intensity. The fit of our model to the data with η equal to 1 is shown as the red dash line. The difference in the model fit to the data is shown in the upper inset. The temperature limits in the inset is ± 1 °C. (B) An anisotropic square-wave waveform was applied to the laser intensity (originally at 0.28 W) with the resulting temperature trace shown in A. The laser was on for 2 ms out of 5 ms resulting in a 60% reduction in the overall laser intensity.

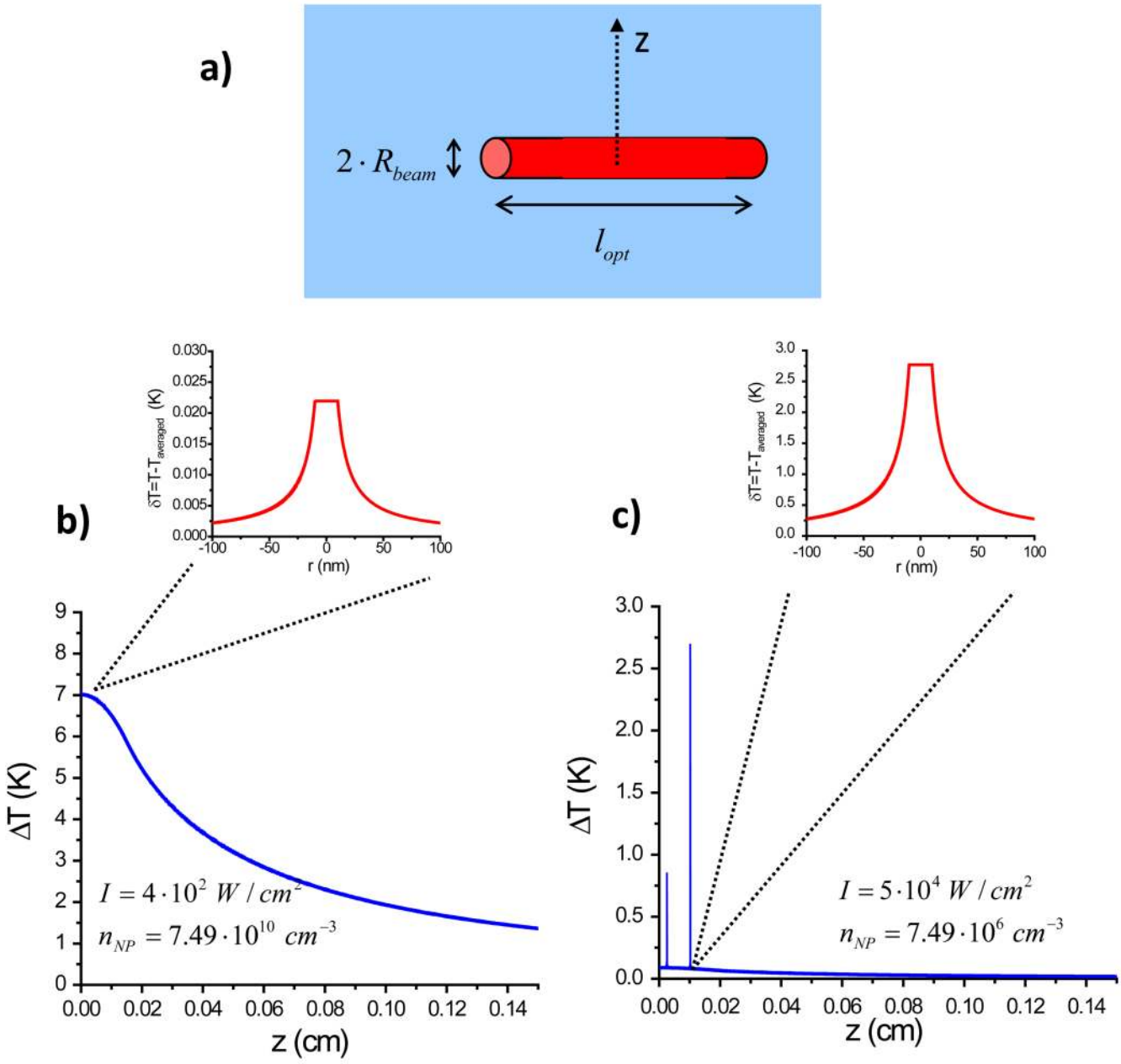

Figure 5.

a) Geometry of the model system with a hot NP cylinder. b) Calculated temperature increase on the mm-scale in the vicinity of the heated cylindrical region. The parameters are similar to those in the experiment. The light power is like in the experiment, moderate; the photon energy is equal to the plasmon peak energy. Here we zoom on a nano-scopic region in the vicinity of a single NP, δT, relative to the local averaged temperate to show a small temperature "bump" of a single NP; $I = 4 \cdot 10^2 W/cm^2$, $n_{NP} = 7.49 \cdot 10^{10} cm^{-3}$. c) The same for the case of a very diluted NP solution and a very high laser power; $I = 5 \cdot 10^4\ W/cm^2$, $n_{NP} = 7.49 \cdot 10^6\ cm^{-3}$. We see now very sharp "spikes" in the temperature profile due to optically-driven single NPs. Such hot spots can be created and studied using single-NP spectroscopy.[10] Again we zoom on a region in the vicinity of a single NP.